Electronic Supplementary Information

Lattice-strain Effects on the Electronic Structure and Magnetism in Epitaxial $SmCrO_3$ Thin Films

Mohit Madaan[1], Prachi Gurawal[2], Rinku Kumar[3], Anil Jain[4,5], Abhishek Nag[1*], Vivek K. Malik[1*]

[1] *Department of Physics, Indian Institute of Technology Roorkee, Roorkee 247 667, India*

[2] *Institute Instrumentation Centre, Indian Institute of Technology Roorkee, Roorkee 247 667, India*

[3] *Department of Physics, Maitreyi College, University of Delhi, New Delhi 110 021, India*

[4] *Solid State Physics Division, Bhabha Atomic Research Centre, Mumbai 400 085, India*

[5] *Homi Bhabha National Institute, Anushaktinagar, Mumbai 400 094, India*

* Corresponding author: vivek.malik@ph.iitr.ac.in , abhishek.nag@ph.iitr.ac.in

Polycrystalline $SmCrO_3$ (SCO) synthesis by solid-sate reaction method:

Polycrystalline sample of SCO was prepared via conventional solid-state reaction procedure with oxide precursors (99.99 % purity) Cr_2O_3 and Sm_2O_3 from Sigma Aldrich. The constituent oxide precursors in appropriate stoichiometric proportion (Sm: Cr =1:1) were mixed, after pre-heating to remove any moisture and then ground in an agate mortar with a small amount of acetone. Upon complete evaporation of the acetone, the mixture was compacted and calcined at required temperatures, with intermediate grinding. X-ray diffraction analysis, performed after each grinding step, confirmed the sequential synthesis of the single-phase orthorhombic SCO. Once the well-mixed pure phase was obtained, 5% polyvinyl alcohol (PVA) binder was added and mixed, then ground to get a fine powder. Subsequently, the fine powder was pressed into a dense pellet followed by sintering at 1200 °C for several hours, for using as a target in a PLD chamber for the thin film growth.

The crystal structure of SCO is investigated using Rigaku Miniflex benchtop X-ray diffractometer in a Bragg's angle range. It is evident from Rietveld refinement that SCO crystalizes in orthorhombic perovskite structure. After final-refinement cycle, Cr atoms are located at 4*b* Wyckoff site, Sm-atoms and axial oxygen (O1) occupy 4*c* site while equatorial oxygen (O2) is positioned at 8*d* general Wyckoff site, with four molecular formula units per cell. Refined parameters are summarized below in **Table I.**

Table I. Structural parameters for polycrystalline $SmCrO_3$ after Rietveld refinement.

Crystal structure	Orthorhombic
a(Å)	5.3664(6)
b(Å)	5.4994(7)
c(Å)	7.6445(4)
$\alpha = \beta = \gamma$	90°
Sm 4*c*(x, y, ¼)	(-0.01108, 0.05022, ¼)
Cr 4*b*(½, 0, 0)	(½, 0, 0)
O1 4*c*(x, y, ¼)	(0.06288, 0.48854, ¼)
O2 8*d*(x, y, z)	(0.48929, 0.29951, 0.04576)

Structural and magnetic properties of additional epitaxial SCO/(001) LSAT thin film:

Below are the structural and magnetic characterization of another PLD-grown SCO film on (001) LSAT substrate to compare with SCO film on (001) STO. During the deposition, same optimized growth parameters were maintained as for the SCO/STO film discussed in main manuscript.

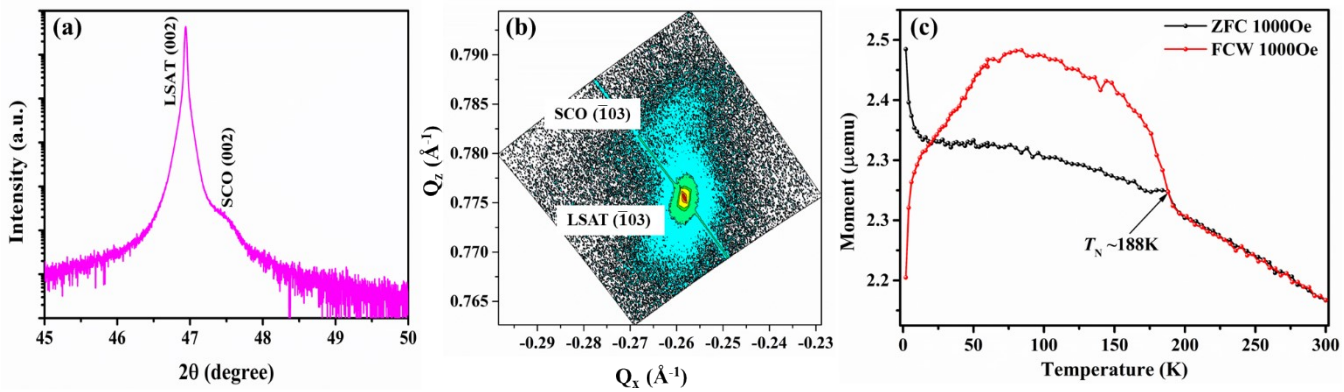

Fig. S1. The epitaxial nature of the SCO/LSAT film. (a) Enlarged 2θ-ω scan around (002) reflection. (b) Asymmetric RSMs around the (1 $\bar{0}$3) reflection, and (b) Magnetization vs. temperature curves for SCO/LSAT. The Néel temperature is estimated at the ZFC-FC bifurcation.

FE-SEM analysis of polycrystalline and thin-film SCO:

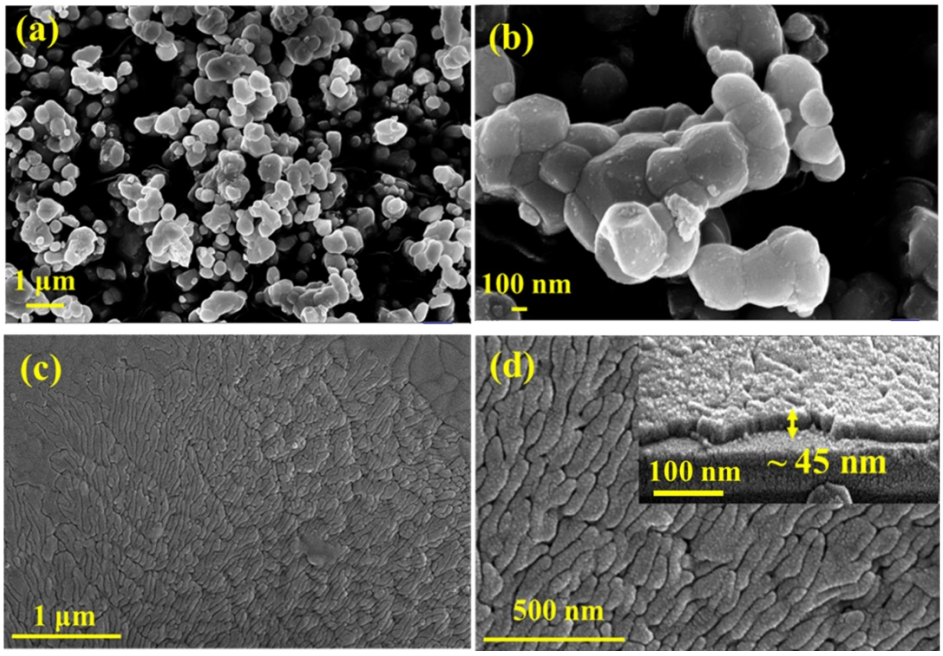

Fig. S2. FE-SEM micrographs for polycrystalline $SmCrO_3$ at (a) low and (b) high magnifications, and for $SmCrO_3$ thin film (c) & (d) display top-view surface images on (Si-substrate), with inset of (d) showing cross-section with an average film thickness of 45 nm.

XPS analysis:

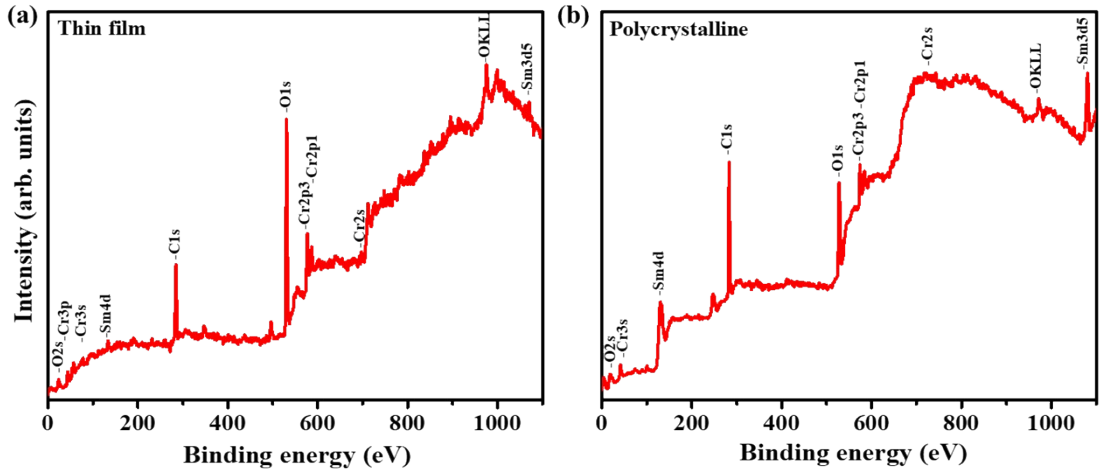

Fig. S3. Survey scan spectra of (a) thin film and (b) polycrystalline SCO.

Tauc plot analysis for SCO/Sapphire

To ensure a reliable experimental reference in parallel with the available literature on bulk SCO, we have deposited an SCO film on sapphire substrate. Owing to the optically transparency in SCO's relevant spectral region (wide band gap of ~9 eV), sapphire enables precise optical measurements while supporting polycrystalline growth. UV–vis spectroscopy for the SCO/sapphire film was performed using UV-1800, Shimadzu UV spectrophotometer over the wavelength range 250-900 nm. The optical band gap determined from Tauc's plot of the transmission spectra is ~3.4 eV, consistent with ellipsometry-derived value.

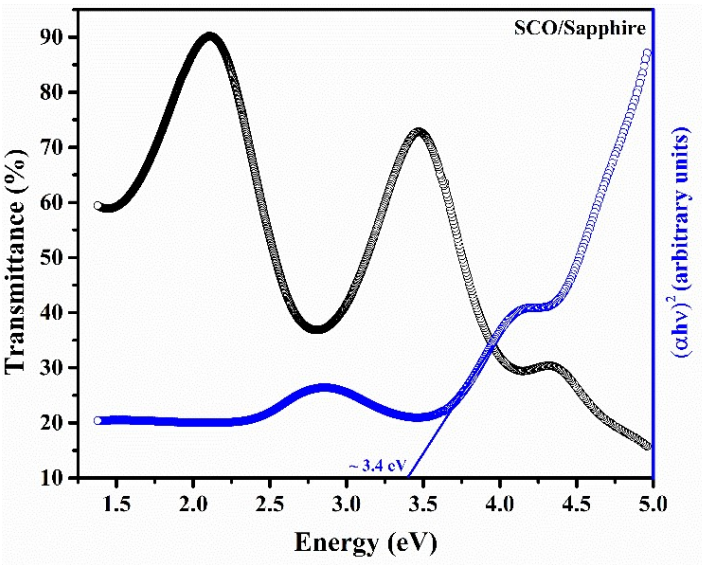

Fig. S4. Transmittance spectrum and Tauc's plot for polycrystalline SCO/sapphire.

These results are in excellent agreement with the reported bulk reference from UV-vis studies, where polycrystalline $SmCrO_3$ exhibits a band gap in the range 3.28–3.397 eV. This establishes the SCO/sapphire film as a reliable bulk-like thin-film reference."

UV-vis absorbance analysis for bare STO and SCO/STO thin film:

To highlight the intrinsic absorption of SCO thin film near the STO absorption edge (~3.2 eV), UV-absorbance spectra for both bare STO and the strained SCO/STO thin-film were measured.

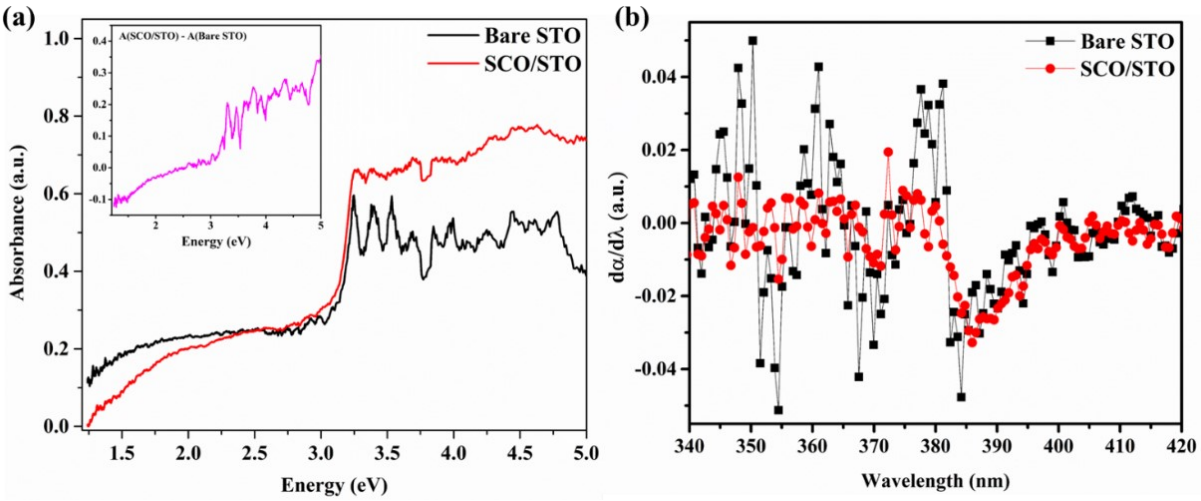

Fig. S5. (a) Normalized UV-vis absorbance spectra with substrate-subtracted inset, and (b) derivative spectra of bare STO and SCO/STO.

Compared to STO substrate, the SCO/STO film exhibits an additional absorbance near the edge (Fig. S5a), indicating a distinct contribution from the SCO layer. Further, after substrate-subtraction, a weak film-related absorption corresponding above the STO edge becomes apparent (inset of Fig. S5a), as expected for a thin (~ 45 nm) film, though it remains relatively small compared to the strong STO absorption in this region.

In addition, derivative ($d\alpha/d\lambda$) analysis further reveals a smoother and slightly shifted feature relative to STO, as shown in Fig. S5b. Importantly, the UV–vis absorbance and substrate-subtracted spectra in this approach provide clear signature of the SCO contribution above the STO absorption edge. Despite the strong substrate absorption, these features indicate an intrinsic band gap near ~3.3 eV, in good agreement with ellipsometry analysis.

AC magnetic susceptibility of SCO/STO film:

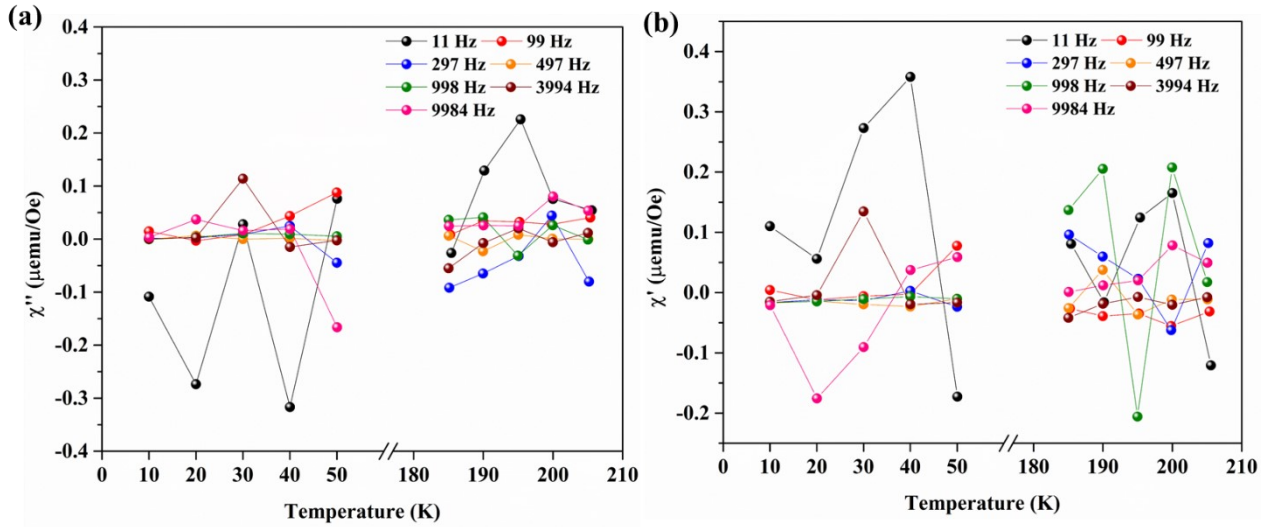

Fig. S6. Frequency dependence (11 Hz – 9984 Hz) of (a) real (χ′) and (b) imaginary (χ″) AC response in transition regions.